J Solid State Electrochem (2007) 11:1163–1169
DOI 10.1007/s10008-006-0256-2

ORIGINAL PAPER

Electrochemical impedance spectroscopy of mesoporous Al-stabilized TiO_2 (anatase) in aprotic medium

Adel Attia · Marketa Zukalova · Lubomir Pospisil · Ladislav Kavan

Received: 22 June 2006 / Revised: 23 November 2006 / Accepted: 8 December 2006 / Published online: 16 January 2007

Abstract High-frequency electrochemical impedance spectroscopy was used to investigate the mesoporous film of Al-stabilized TiO_2 on F-doped SnO_2 support in 1 M Li $(CF_3SO_2)_2N$ in ethylene carbonate/dimethoxyethane (1:1 *v*/*v*). Kinetic parameters, viz. charge transfer resistance and chemical diffusion coefficient, were determined. Charge transfer resistance increased with time of contact of electrode in the above aprotic electrolyte solution. The increase followed exponential dependence, whereas the double layer capacitance, simultaneously, decreased exponentially with time. These effects were discussed in terms of the solid–electrolyte interface, which undergoes chemical changes upon contact with the electrolyte solution.

Keywords Impedance spectroscopy · Solid–electrolyte interface · Titanium dioxide · Anatase · Lithium insertion

Adel Attia is currently on leave from the Department of Physical Chemistry, National Research Center, El-Tahrir St., Dokki 12622, Cairo, Egypt.

A. Attia (✉) · M. Zukalova · L. Pospisil · L. Kavan
J. Heyrovský Institute of Physical Chemistry,
Academy of Sciences of the Czech Republic,
Dolejškova 3,
182 23 Prague 8, Czech Republic
e-mail: adel_attia@hotmail.com

Present address:
A. Attia
State Key Lab for Physical Chemistry of Solid Surfaces,
Department of Chemistry, Xiamen University,
Xiamen 361005, China

Introduction

Anatase TiO_2 electrodes find application in solar cells, lithium ion batteries, and electrochromic devices [1–3]. Due to its good Li-storage capacity, cycling stability, and safety against overcharging [4], nanocrystalline TiO_2 (anatase) represents a promising electrode material for Li-ion batteries. Aluminum is known to stabilize the titania matrix, but it does not contribute to the electrochemical accommodation of lithium due to the fixed valence of Al^{3+}. Hence, the specific faradaic capacity of the Al_2O_3/TiO_2 system for Li-insertion is smaller than that of pure TiO_2 [5–7]. Nevertheless, Al and other doping metals in Li–host structures may influence their electronic properties and, thus, improve the voltage and other electrochemical characteristics of the electrode materials [8].

There has been accordingly considerable interest in Al doping of ternary oxides, $LiMO_2$ (M is a metal), which are active for lithium storage. Theoretical and experimental studies confirm that Al substitution of the transitional metal cation increases the cell voltage [9]. Ohzuku et al. [10] demonstrated this effect for Al doping in layered $LiNiO_2$. Jang et al. [11] observed that the open circuit potential (OCP) of $LiAl_yCo_{1-y}O_2$ increased systematically with increasing content of Al, and there was also an improvement in lithium diffusivity, cycle life, and charge capacity. Chen and Dahn [12] studied $LiCoO_2$ covered by ZrO_2, Al_2O_3, and SiO_2 and have found that Al_2O_3-coated $LiCoO_2$ exhibited the best cycle life.

Aluminum was found to be crucial for stabilization of the anatase lattice during chemical transport reactions in the TiO_2–$TeCl_4$ systems, and a large anatase single crystal could only be grown with the aid of Al stabilization [13]. A special form of mesoporous alumina has been frequently used as a template for the fabrication of anatase nanotubes

and nanowires [14–18]. Zhang and Banfield [19] reported that the anatase to rutile phase transformation retarded to higher temperatures by the addition of Al_2O_3 to anatase TiO_2. A similar effect was also traced for zirconia in anatase [2]. In our previous works [20, 21], the Al-stabilized anatase was shown to exhibit smaller particle size and larger Li-diffusion coefficient than the reference Al-free anatase. Hence, our Al–TiO_2 material turns to be particularly suitable for investigation of effects occurring at the electrode surface, such as the formation of solid–electrolyte interface (SEI).

The SEI is essential for the action of graphite anodes, but it is also formed at oxidic Li–host structures, operating at larger potentials than graphite [22, 23]. In the case of Al–TiO_2, the lattice distortion and core-shell morphology played an important role affecting the electrochemical properties. In the present work, our earlier investigation of these electrode materials has been upgraded by employing electrochemical impedance spectroscopy (EIS). We have selected for this study the most promising Al–TiO_2 material, having the largest Brunauer–Emmett–Teller (BET) surface area, and superior Li-insertion kinetics from cyclic voltammetry (CV; for details see Refs. [20, 21]).

Experimental

Materials

The synthesis of Al-stabilized titania followed the same protocol as described previously [20, 21]. The solution of Keggin cations $Al_{13}O_4(OH_{24})^{7+}$ was prepared by dissolving 13.13 g of $AlCl_3{\cdot}6H_2O$ in 420 ml of water, and the pH was adjusted to 3.95 with concentrated ammonium hydroxide. The solution of Ti precursor was prepared by mixing 4.54 g of $(NH_4)_2Ti(OH)_2(C_3H_2O_3)_2$ (Tyzor LA, DuPont) and 8.82 g cetyltrimethylammonium chloride (CTAC, Lonza). Then, 66.18 ml of the solution of Keggin cations was diluted to 80 ml with water and added slowly at vigorous stirring to the Tyzor/CTAC mixture. A white precipitate, which formed immediately, was aged in a Teflon bomb at room temperature overnight, at 70 °C for 1 day, and at 100 °C for 2 days, and subsequently isolated by washing and centrifuging. Finally, the material was calcined at 450 °C for 3 h. A reference Al-free blank material was prepared in the same way, but the addition of the solution of Keggin cations was omitted. The final Al-modified TiO_2 contained 9.6 wt.% of Al_2O_3 and exhibited the BET surface area of 185 $m^2\ g^{-1}$. This value compares favorably to the BET surface area of a blank Al-free TiO_2 (73 $m^2\ g^{-1}$) prepared by the same synthetic protocol without Al addition.

Preparation of electrodes

The electrodes were prepared similarly to that in Refs. [2, 3] by using CH_3COOH and Triton X-100 as dispersing agent and surfactant, respectively. The powder material was dispersed into a paste by slow mixing with 0.1 M CH_3COOH under continuous grinding in agate mortar. After about 20 min of homogenization, the slurry was mixed with Triton X-100 and further homogenized. The SnO_2(F)-coated glass from Nippon sheet glass, 10 Ω/square, served as a support for the electrode preparation. The Al–TiO_2 electrode was prepared by a doctor blade method. Scotch tape placed at the edge of the support defined the film thickness and left part of the support uncovered for electrical contact. The geometrical area was defined by masking with Scotch tape at the glass edges and was 0.385 cm^2 in all experiments. The electrode was finally calcined for 3 h in air at 450 °C. Stylus profilometry and scanning electron microscopy evidenced that the thickness of the electrode film was around 1 μm.

Characterization

X-ray diffraction was studied on a powder material using a Siemens D-5005 diffractometer in the Bragg–Brentano geometry with CuKα radiation. EIS measurements were carried out in a one-compartment cell using Hewlett-Packard 4192A gain phase impedance analyzer. The freshly immersed electrode was first subjected to one CV scan starting from the OCP and progressing as follows: OCP → 3 V → 1.1 V → 3 V (all potentials vs Li/Li^+). At this stage, the working electrode was disconnected, relaxed at OCP for a defined time, and the EIS

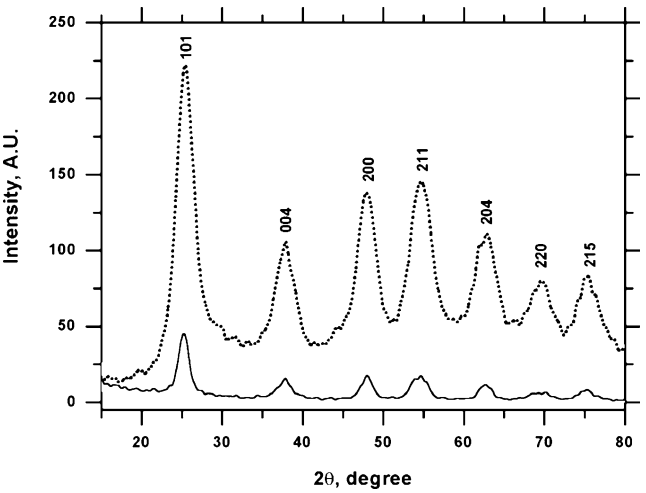

Fig. 1 Powder X-ray diffraction patterns of Al–TiO_2 (*dashed line*) compared to blank sample (*solid line*) prepared by the same synthetic method and with no addition of Al precursor. The Miller indices of the Bragg peaks are indicated near each peak

measurements followed. The impedance measurements (from 12 MHz to 5 Hz) were carried out at open circuit voltage. The time of contact was measured from the completion of the cyclovoltammetric experiment until the start of the EIS measurement. Non-linear fitting and physical modeling of the data were performed by using Equivcrt software version 4.55 (Equivcrt, "Equivalent Circuit") developed by Boukamp [24]. The time interval between each EIS measurement was 10 min. This makes the electrode time exposure to the electrolyte minimum at the beginning. Both the reference and auxiliary electrodes were from Li metals. $LiN(CF_3SO_2)_2$ (Fluorad HQ 115 from 3 M) was dried at 130 °C/1 mPa. Ethylene carbonate (EC) and 1,2-dimethoxyethane (DME) were dried over the 4-Å molecular sieve (Union Carbide). The electrolyte solution, 1 M $LiN(CF_3SO_2)_2$+EC/DME (1:1 *v*/*v*), contained 15–40 ppm H_2O as determined by Karl Fischer titration (Metrohm 684 coulometer). All operations were carried out under argon atmosphere in a glove box.

Results and discussion

Characterization of electrodes

Figure 1 shows the powder X-ray diffractogram of the electrode material compared to that of the reference material obtained by the same synthetic route but without addition of Al (see "Experimental" section). All peaks can be indexed as anatase phase only. Although a solid solution between alumina and titania was reported to form above 1,000 °C [25], the formation of such a species is improbable at our experimental conditions. The coherent domain size was about 3 nm, as calculated from the X-ray line broadening (Scherrer formula) [26]. The presence of a thin layer of rutile on TiO_2 (anatase) core was detected by micro-Raman spectroscopy on the Al-containing sample (data not shown). The layer is obviously too thin to be detectable by X-ray diffraction [20, 21]. These results confirm our previously reported data [20, 21] on almost identical samples.

Electrochemical impedance spectral analysis

Steady-state ac-impedance measurements are more reliable than pulse techniques where cathodic pulses can increase the surface lithium concentration to or even beyond the limiting composition of the electrode. In such a case, any measurable diffusion could arise from different processes. A surface layer formed on the electrode due to decomposition of the electrolyte may influence the insertion of Li^+ into the host material. The formation of solid electrolyte interface on TiO_2 has not been systematically investigated yet. However, there is typically about 4–9% of irreversible charge during the first cycle(s) of Li-insertion into TiO_2 (anatase) [3, 26] that is reminiscent of the SEI formation on other oxidic materials, such as $LiMn_2O_4$ [23]. In addition to this, the slight charge irreversibility of Li-insertion at the time scale of CV may also indicate small retention of Li^+ inside the anatase lattice after completing the CV scan [3, 26]. The Li-ion transport through the SEI, as well as the residual Li, should consequently be considered for understanding of the electrochemical data in general and the EIS in particular.

Figure 2 (curves a–g) shows typical Nyquist plots obtained for the Al-doped mesoporous anatase electrode, which were immersed for different times in the electrolyte at OCP. Impedance spectrum during the first 10 min of immersion time was instable in time; hence, the values were not considered for data fit using the Equivcrt software [24]. The impedance spectra consisted of two separated arcs, one at the ultrahigh and the other at high-frequency ranges. The

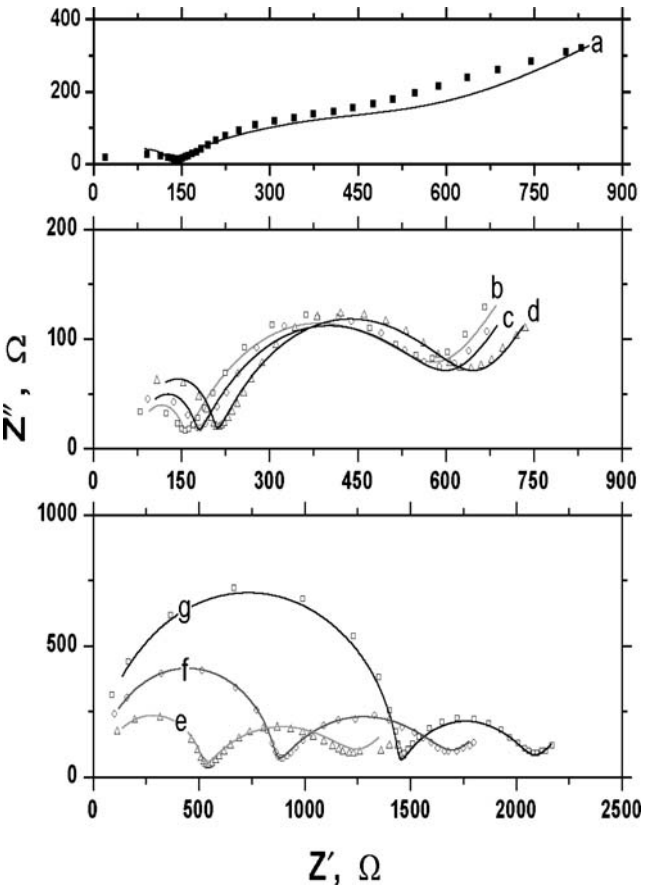

Fig. 2 Impedance measurements represented in Nyquist form of Al–TiO_2 electrode in 1 M $Li(CF_3SO_2)_2N$ in EC/DME (1:1 by mass). The lowest frequency was 5 Hz. The electrode immersion time in the electrolyte solution was 20, 30, 40, 50, 60, 70, and 80 min for *curves a–g*, respectively. *Solid line* represents fitting, whereas *markers* represent the experimental data

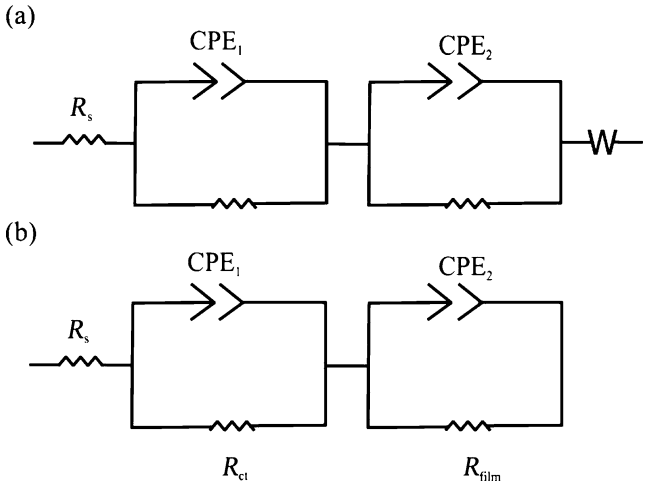

Fig. 3 Equivalent circuit used for analysis of high-frequency electrochemical impedance spectroscopy of Al–TiO_2 electrode (**a** with linear part, **b** without linear part)

low frequency data inclined to a straight line with a slope of approximately 45 °. The impedance spectra of Al–TiO_2 electrode at different times of contact with the electrolyte solution exhibited a typical behavior of a blocking electrode at the minimum time of immersion. In general, the presence of the second semicircle indicates a response of grain interior–grain boundary phase system [27]. The spectrum showing a response at the whole frequency range may be regarded as an imperfect semicircle (Fig. 2, curve a). This indicates that the electrode behaves as having a high polarization resistance, which may be caused by a larger interface impedance and charge accumulation on the surface.

It is likely that the Li^+ desolvation before its interaction with the electrode material is involved in the observed high polarization resistance. The early work of De Levie [28] showed that, for porous electrodes, the phase angle of the impedance is half of that of the equivalent flat electrode and that the absolute magnitude of the impedance of a porous electrode is proportional to the square root of the value equivalent to a flat electrode. De Levie's conclusion, indeed, applies to our spectrum (Fig. 2, curve a). Other models leading to depressed complex impedance plot were also considered [29, 30], but they do not seem to be suitable for our case (*vide infra*).

The electrochemical impedance spectra at Fig. 2, curves b–d, contains two semicircles and a short linear part at the lowest frequency. The only difference between both spectra is the time of immersion. The diameter of the first semicircle increased with the time of immersion. Figure 2, curves e–g, demonstrates that the diameter increase is manifested well in the semicircle at ultrahigh frequency, whereas the diameter of the second semicircle at high-frequency region decreases. The linear part started to decline by increasing the time of electrode immersion (Fig. 2, curves a–e). In this case, the impedance is dominated by the electron transfer resistance.

Figure 3a shows the equivalent circuit, which was used to fit experimental impedance spectra of Al–TiO_2 at different time interval of immersion. It is a serial combination of the solution resistance R_s, two parallel circuits, and a Warburg mass transfer impedance. Each of the parallel circuits contains a constant phase element and a parallel resistor. Element CPE_1 reflects the behavior of the double layer capacitance to which is connected a parallel charge transfer resistance R_{ct}. The other circuit containing CPE_2 and R_{film} represents the capacity of the surface film and the rate of electron transfer across it (expressed as R_{film}). This circuit describes well the impedance spectra with two semicircles and a linear part (as shown in spectra b, c, and d of Fig. 2). Table 1 shows the fitting parameters used. It describes the impedance spectra with two semicircles and a linear part (corresponding to spectra b, c, and d in Fig. 2). Both parallel circuits are connected to W in series that is related to the Warburg diffusion impedance.

Table 1 Fitting parameters for the proposed equivalent circuits

Time (min)	R_s (Ω)	CPE_1-t (F)	CPE_1-p	R_2 (Ω)	CPE_2-t (F)	CPE_2-p	R_3 (Ω)	W-R (Ω)	W-t (s)	W-p	χ^2	Sum of square
20	65.37	1.875E-8	1.306	40.37	0.0014276	0.86764	100.3	1,378	307.2	0.26502	0.02494	3.0934
30	79.62	2.3663E-7	1.031	70.54	6.5121E-4	0.58657	428.3	907.4	862.7	0.5	0.00325	0.39996
40	81.24	1.64E-7	1.042	89.1	6.53E-4	0.58024	428.9	1,383	3,024	0.5	0.00251	0.30911
50	81.58	1.54E-7	1.018	121	6.081E-4	0.5994	439.2	1,620	4,127	0.5	0.00142	0.17197
60	49.87	7.08E-8	1.013	457.7	3.74E-4	0.59343	750.6	N/A	N/A	N/A	0.00173	0.17677
70	48.61	4.44E-8	1.049	781	3.47E-4	0.57765	916.3	N/A	N/A	N/A	0.00126	0.13569
80	37.63	4.65E-8	1.035	1,384	4.36E-4	0.67509	706.1	N/A	N/A	N/A	9.64E-5	0.09543

χ^2 and sum of square are the fitting parameters.

R_s Electrolyte resistance, *CPE_1-t*/*CPE_1-p* elements of constant phase element (magnitude and exponent parts, respectively) at high frequency range, R_2 charge transfer resistance, *CPE_2-t* and *CPE_2-p* elements of constant phase element (magnitude and exponent parts, respectively) at lower frequency range, R_3 resistance of electron transfer across the electrode film, *W-R*/*W-t*/*W-p* elements of Warburg impedance associated to chemical diffusion into the electrode material

The second equivalent circuit, Fig. 3b, is almost the same as that aforementioned in Fig. 3a. It is solely characterized by the absence of linear part. This equivalent circuit describes well the spectra e, f, and g in Fig. 2, which have two semicircles with a small linear part. In this study, CPE_1 represents again the double layer capacitance, whereas CPE_2 stands for a charge accumulation process caused by a slow interfacial process in which guest ions incorporate from the electrolyte into the surface film and, eventually, into the host lattice. The constant phase element is connected with the surface distribution of the interfacial capacitance, which showed that the frequency dispersion can be a property of the double layer itself. In this study, the dominant process is the interaction of Li^+ with the surface structure. Therefore, we consider our model to be similar to that in Ref. [29] for an irreversible reaction. In the present case, the "ladder network" consists of only two parallel circuits connected in series. This phenomenon is more common in the case of intercalation electrodes, which can be described by an adsorption capacitance, C_{ad}, in parallel with $R_{lattice}$ incorporated ions to lattice [31]. The two arcs in the higher-frequency range are due to reactions at the electrolyte/electrode interface, and the inclined line in the lower-frequency range is attributed to a Warburg diffusion impedance through the electrode. However, as it was mentioned before, the second semicircle may be considered as a charge accumulation caused by a slow interface process in which guest ions incorporate from electrolyte into the electrode material [31]. We suggest that the reverse process can occur analogously. It can be represented by the same equivalent circuit, i.e., desorption capacitance, C_{des}, in parallel to resistance, $R_{lattice}$, due to extraction of incorporated ions from the electrode material. Conway [32] gave an evidence for the close resemblance between the adsorption and intercalation processes derived from fundamental thermodynamics.

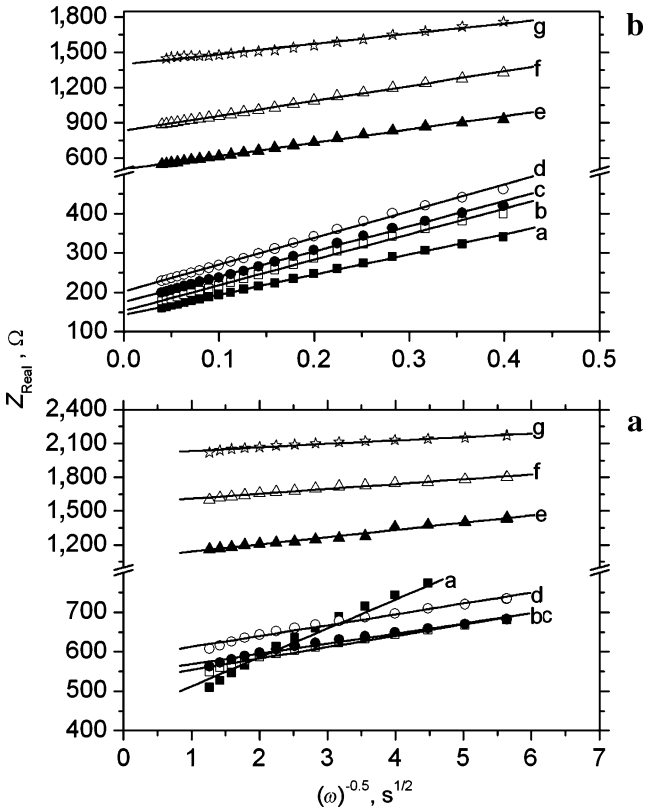

Fig. 4 Real part of impedance as a function of $\omega^{-0.5}$ for **a** low angular frequencies and **b** high angular frequencies. At each graph, the *curves a*, *b*, *c*, *d*, *e*, *f*, and *g* represent the time of contact of 20, 30, 40, 50, 60, 70, and 80 min, respectively

It is reported elsewhere [33] that low-frequency CPE can influence the diffusion modeling due to change of the value of the diffusion coefficient by two orders of magnitude. Due to this influence, we determined the diffusion coefficient by an alternative method. Nonetheless, the capacitive behavior of CPE at low frequencies can be attributed to back contact. However, this could not be considered true, as Warburg and CPE exponents should be proportional [34].

Figure 4a, b presents the dependence of the real part of impedance on $\omega^{-0.5}$. The plot shows, separately, high- and low-frequency dependencies (the minimum was 5 Hz). Charge transfer resistance was determined from the intercept of the straight lines at different contact time, whereas the slope of the lines was used for determination of the diffusion coefficient according to the following equations:

$$R = R_s + R_{ct} + \frac{\sigma}{\omega^{1/2}} \tag{1}$$

$$\sigma = \frac{R_g T}{A(2D)^{1/2}(nF)^2\left(\frac{1}{C_O^\infty} + \frac{1}{C_R^\infty}\right)} \tag{2}$$

where R is the real part of impedance, R_s is the solution resistance, R_{ct} is the charge transfer resistance, σ is the Warburg coefficient, ω is angular frequency, R_g is the universal gas constant, T is absolute temperature, A is the geometrical area of the electrode (0.385 cm^2, see "Experimental" section), D is the chemical diffusion coefficient of Li^+ into the Al–TiO_2 film, and from it, n is the number of electrons, F is Faraday constant, and C_O^∞ and C_R^∞ are the concentrations of oxidized and reduced species, respectively.

The plot of Z_{Real} vs $\omega^{-0.5}$ yields σ as the slope and $R_{ct}+R_s$ as the intercept. Substituting σ in Eq. 2, we get the chemical diffusion coefficient, D. The obtained value was $(2.1\pm0.5)\times10^{-16}$ cm^2 s^{-1} at high frequencies, whereas at low frequencies it corresponded to a value of $(3.6\pm0.9)\times10^{-19}$ cm^2 s^{-1}. The D value determined from the plot in Fig. 4 is comparable to the value obtained by using the linear part of impedance (Warburg impedance); however,

the values are closer in the case of lower-frequency range, whereas the values at higher frequency are more realistic ones. There is a good correlation between the values obtained at low- and high-frequency range.

The found values of D at low frequencies obviously can hardly be assigned to the Li diffusion inside the ordinary anatase lattice, whereas the D values at high-frequency ranges match that of nanocrystalline anatase (10^{-14}–10^{-17} cm^2 s^{-1}) of different origins [35–38]. Our actual Al-modified TiO_2 material provided the D value of 6×10^{-17} cm^2 s^{-1} from CV (cf. also Refs. [20, 21]). Due to different time scales, the CV technique is suitable for investigation of the Li transport in the bulk anatase [35–38], whereas the EIS highlights the effects occurring at the electrode surface only. We consequently ascribe the smaller diffusion coefficients at low-frequency EIS to other processes than the Li diffusion in anatase, presumably, to Li-ion transport through the surface films (SEI). We may, alternatively, consider the influence of a rutile shell, which was found on the electrode surface (cf. also Refs. [20, 21]). Although the Li-insertion into rutile was not that systematically studied as that for anatase, the diffusion coefficient of Li^+ in rutile lattice might be comparable or even higher than that in anatase [13]. The ultrasmall D values observed here at low-frequency range would consequently hardly account for the presence of rutile shell. The passivation surface film (SEI) turns to be the only plausible explanation for our EIS data.

Charge transfer resistance

Figure 5 shows the change of charge-transfer resistance and capacitance with time of the electrode/electrolyte solution contact. The squares denote values from the intercept of slopes to Z_{Real}-axis of Fig. 4b (at high frequency). The stars denote values obtained directly from the Nyquist plot (Fig. 2). Both sets of data are obviously well comparable. Open circles are the experimental data obtained at lower frequency from Fig. 4a. The charge transfer resistance increases exponentially with time, albeit the actual values obtained for high and low frequencies exhibit a constant shift. The true capacitance was calculated from the following equation:

$$C = Q^0(\omega_{max})^{n-1} \quad (3)$$

The true capacitance is equal to CPE (its magnitude represented by Q^o in Eq. (3) if n=1, and CPE capacitance properties decreases when n approaches zero, ω_{max} is the frequency at which maximum imaginary impedance attains. The true capacitance is plotted in Fig. 5 against the increase

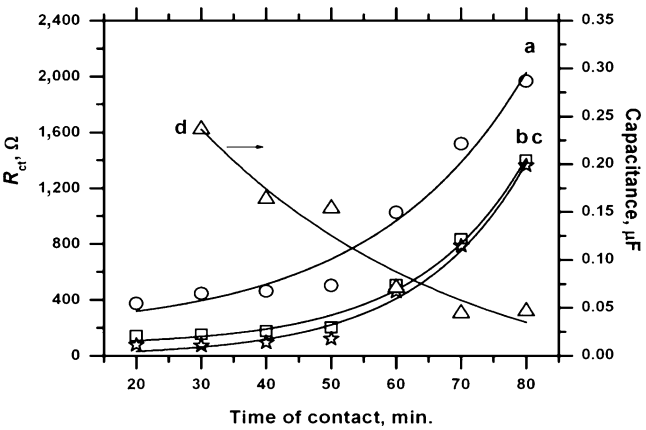

Fig. 5 Charge transfer resistance (R_{ct}) and double layer capacitance changes as a function of the immersion time of Al–TiO_2 electrode in 1 M $Li(CF_3SO_2)_2N$ in EC/DME (1:1 v/v). R_{ct} calculated from **a** lower frequency (extracted from Fig. 4), **b** semicircle intercept with x-axis, **c** high frequency (extracted from Fig. 4), and **d** true double layer capacitance during elapse of time of the electrode immersion in the electrolyte

in the time of immersion and is found to be inversely related to it.

The increase in the charge transfer resistance reflects changes in the electrical properties at the interface, which develops with the time of the electrode/electrolyte solution contact. It is tempting to suggest that these effects are due to the presence of small residual Li^+ inside the anatase lattice after the CV scan (see above). The final potential after the CV scan (3 V) is, obviously, well above the Li-extraction potential. Hence, relaxing of this electrode at OCP may remove traces of Li^+ from the TiO_2 host structure. Attainment of the fully de-lithiated state converts the Al–TiO_2 electrode into an insulating state. As R_{ct} scales inversely with the electrochemical reaction rate, Fig. 5 demonstrates that the reaction rate decreases with time of immersion. This decrease in the rate is attributed to the growth of SEI layer. The formation of SEI is supported by the decrease in double layer capacitance with time of immersion. Our data clearly indicate that the SEI film exhibits changes upon storage in the electrolyte solution at OCP. In this respect, we may recall the SEI chemistry on other oxidic materials, such as $LiNiO_2$ and $LiMn_2O_4$ at similar conditions: In this study, the pristine surface film is initially composed of Li_2CO_3 as the main component but converts gradually to a variety of compounds including ROLi, $ROCO_2Li$, (R = alkyl) polycarbonates, etc. [22]. Understanding the nature of SEI chemistry on Al–TiO_2 is beyond the scope of this paper, but it is clear that the EIS is a particularly suitable technique for in situ monitoring of the changes in SEI, which can hardly be detected by CV and chronoamperometry. These methods do not provide explicit data on the SEI, as they mainly reflect the bulk Li^+ transport in anatase [35–38].

Conclusions

Mesoporous Al-stabilized TiO_2 (anatase) electrode was studied by the EIS. The chemical diffusion coefficient was determined by analyzing the real impedance part vs the square root of reciprocal of angular frequency. In the high-frequency range of the impedance, the chemical diffusion coefficient values determined were close to previously obtained values. However, at the low-frequency range, the values were quite small, which can be assigned to the Li-ion transport through SEI, and are by orders of magnitude smaller than the diffusion coefficients of Li^+ in the bulk anatase lattice. Charge transfer resistance increased with time of immersion of electrode, which we attribute to the formation and gradual reconstruction of the SEI.

Acknowledgment This work supported by the Academy of Sciences of the Czech Republic (contract No. N100500652) and the EC-COST D35.0002 grant.

References

1. Hagfeldt A, Graetzel M (1995) Chem Rev 95:49
2. Kavan L, Attia A, Lenzmann F, Elder SH, Graetzel M (2000) J Electrochem Soc 147:2897
3. Kavan L, Graetzel M, Rathousky J, Zukal A (1996) J Electrochem Soc 143:394
4. Huang SY, Kavan L, Exnar I, Graetzel M (1995) J Electrochem Soc 142:L142
5. Zhong Q, von Sacken U (1995) J Power Sources 54:221
6. Ohzuku T, Ueda A, Kouguchi M (1995) J Electrochem Soc 142:4033
7. Ohzuku T, Yanagawa T, Kouguchi M, Ueda A (1997) J Power Sources 68:131
8. Aydinol MK, Kohan AF, Ceder G, Cho K, Joannopoulos J (1997) Phys Rev B 56:1354
9. Ceder G, Chiang YM, Sadoway DR, Aydinol MK, Jang YI, Huang B (1998) Nature 392:694
10. Ohzuku T, Takehara Z, Yoshizawa S (1979) Electrochim Acta 24:219
11. Jang YI, Huang B, Wang H, Sadoway DR, Ceder G, Chiang YM, Liu H, Tamura H (1999) J Electrochem Soc 146:862
12. Chen Z, Dahn JR (2003) Electrochem Solid-State Lett 6:A221
13. Kavan L, Graetzel M, Gilbert SE, Klemenz C, Scheel HJ (1996) J Am Chem Soc 118:6716
14. Li F, Zhang L, Metzger RM (1998) Chem Mater 10:2470
15. Lin Y, Wu GS, Yuan XY, Xie T, Zhang LD (2003) J Phys Condens Matter 15:2917
16. Matsumuoto Y, Ishikakwa Y, Nishida M, Seiichiro I (2000) J Phys Chem B 104:4204
17. Michailowski A, AlMawlawi D, Cheng G, Moskovits M (2001) Chem Phys Lett 349:1
18. Zhang X, Yao B, Zhao L, Liang C, Zhang L, Mao Y (2001) J Electrochem Soc 148:G398
19. Zhang HZ, Banfield JF (2000) J Mater Res 15:437
20. Attia A, Zukalova M, Rathousky J, Zukal A, Kavan L (2005) J Solid State Electrochem 9:138
21. Attia A, Elder SH, Jirasek R, Kavan L, Krtil P, Rathousky J, Zukal A (2001) Stud Surf Sci Catal 135:361
22. Aurbach D, Gamolsky K, Markovsky B, Salitra G, Gofer Y, Heider U, Oesten R, Schmidt M (2000) J Electrochem Soc 147:1322
23. Zhang SS, Xu K, Jow TR (2002) J Electrochem Soc 149:A1521
24. Boukamp BA (1986) Solid State Ionics 20:31
25. Goldberg D (1968) Rev Int Hautes Temp Refract 5:181
26. Kavan L, Kratochvilova K, Graetzel M (1995) J Electroanal Chem 394:93
27. Li H, Huang X, Chen L (1998) Electrochem Solid-State Lett 1:241
28. De Levie R (1964) Electrochim Acta 9:1231
29. Brug GJ, van den Eden ALG, Sluyters-Rehbach M, Sluyters JH (1984) J Electroanal Chem 176:275
30. Retter U, Widmann A, Siegler K, Kahlert H (2003) J Electroanal Chem 546:87
31. Li H, Huang X, Chen L (1999) J Power Sources 81–82:340
32. Conway BE (1993) Electrochim Acta 38:1249
33. Liu P, Wu H (1995) J Power Sources 56:81
34. Bisquert J, Garcia-Belmonte G, Bueno P, Longo E, Bulhoes LOS (1998) J Electroanal Chem 452:229
35. Lindstroem, Soedergen S, Solbrand A, Rensmo H, Hjelm J, Hagfeldt A, Lindquist SE (1997) J Phys Chem B 101:7710
36. van de Krol R, Goossens A, Schoonman J (1999) J Phys Chem B 103:7151
37. Cantao MP, Cisnero JI, Torresi RM (1994) J Phys Chem 98:4865
38. Kavan L, Rathousky J, Graetzel M, Shklover V, Zukal A (2000) J Phys Chem B 104:12012